Supplemental Material: Characteristics of Two-Dimensional Quantum Turbulence in a Compressible Superfluid

T. W. Neely,[1,*] A. S. Bradley,[2,†] E. C. Samson,[1] S. J. Rooney,[2] E. M. Wright,[1] K. J. H. Law,[3] R. Carretero-González,[4] P. G. Kevrekidis,[5] M. J. Davis,[6] and B. P. Anderson[1,‡]

[1]*College of Optical Sciences, University of Arizona, Tucson, AZ 85721, USA*
[2]*Jack Dodd Centre for Quantum Technology, Department of Physics, University of Otago, Dunedin 9016, New Zealand*
[3]*Mathematics Institute, University of Warwick, Coventry CV4 7AL, UK*
[4]*Department of Mathematics and Statistics, San Diego State University, San Diego, CA 92182, USA*
[5]*Department of Mathematics and Statistics, University of Massachusetts, Amherst, MA 01003, USA*
[6]*School of Mathematics and Physics, University of Queensland, Brisbane, Qld 4072, Australia*

Here we provide material supplementing the main text "Characteristics of Two-Dimensional Quantum Turbulence in a Compressible Superfluid." The supplemental material consists of additional description of numerical and experimental methods, five figures, and a movie.

Theoretical background. The damped GP theory used in our simulations can be derived rigorously for the dilute-gas BEC through a detailed treatment of reservoir interactions within the Wigner phase-space representation [39], by neglecting thermal noise. An approximate and practical stochastic Gross-Piteavskii theory can be obtained [40] by: (i) neglecting the particle-conserving reservoir interaction processes (*scattering* terms) that are known to be small in the quasi-equilibrium regime [41]; and (ii) neglecting the weak spatial and time dependence of the damping parameter. This allows the damping parameter to be calculated *a priori*, once the reservoir parameters are known. The resulting stochastic projected Gross-Pitaevskii equation (SPGPE) has been used to study spontaneous vortex formation [27,40] during Bose condensation, vortex dynamics at high temperature [19,42], and the onset of quasi-condensation in elongated systems [43]. The SPGPE is derived by treating all atoms above an appropriately chosen energy cutoff $\epsilon_{\rm cut}$ as thermalized (incoherent region) with temperature T and chemical potential μ, leading to a grand-canonical description of the atoms below $\epsilon_{\rm cut}$ (coherent region). A dimensionless rate $\gamma \equiv \gamma(T, \mu, \epsilon_{\rm cut})$ describes Bose-enhanced collisions between thermal reservoir atoms and atoms in the coherent region containing the BEC.

However, it is not known how to extract a well-defined condensate orbital from the SPGPE trajectories in high-temperature systems containing vortices. Moreover, extracting the incompressible energy spectrum associated with quantum vortices is challenging in the presence of significant thermal noise. However, both qualitative information about vortex dynamics and kinetic energy spectra can be computed from the damped projected Gross-Pitaevskii equation (DPGPE), obtained by neglecting the noise in the SPGPE. Taking this approach we arrive at a tractable, microscopically determined equation for the condensate wavefunction $\psi(\mathbf{r}, t)$, with *a priori* determined reservoir parameters:

$$i\hbar\frac{\partial\psi(\mathbf{r},t)}{\partial t} = (1 - i\gamma)(L - \mu)\psi(\mathbf{r}, t), \tag{1}$$

where the operator L, defined by

$$L\psi(\mathbf{r}, t) \equiv \left(-\frac{\hbar^2}{2m}\nabla^2 + V(\mathbf{r}) + g|\psi(\mathbf{r}, t)|^2\right)\psi(\mathbf{r}, t), \tag{2}$$

is the generator of GP equation evolution for atoms of mass m in an external potential $V(\mathbf{r})$. The interaction parameter is $g = 4\pi\hbar^2 a/m$, for s-wave scattering length a. In most cases the damping parameter is small ($\gamma \ll 1$), and damping rates are typically much smaller than any other rates that characterize the evolution. This approach has been shown to reproduce the qualitative dynamics of quantum vortices in this experiment [44], and allows direct extraction of quantities useful for characterizing 2DQT.

With the measured total atom number N and temperature T, we use an efficient Hartree-Fock scheme for determining the chemical potential $\mu(N, T)$ and reservoir cutoff energy $\epsilon_{\rm cut}(N, T)$ [42], adapted to the present experiment by accounting for the shift in the trap minimum caused by the central barrier. In applying our approach to modeling the experiment of the main text, we find the self-consistent parameters $\mu = 34\hbar\bar{\omega}$, $\epsilon_{\rm cut} = 83\hbar\bar{\omega}$, for geometric mean $\bar{\omega} = (\omega_r^2\omega_z)^{1/3}$, to describe a system of $N = 2.6 \times 10^6$ atoms held at temperature $T = 0.9T_c$ in the combined trap, giving the damping parameter $\gamma = 7.96 \times 10^{-4}$. The central Gaussian barrier is characterized by half-width $\sigma_0 = 16.3\,\mu$m, and is well contained within the coherent region: $\sigma_0 \ll R_{\rm cut} = \sqrt{2\epsilon_{\rm cut}/m\omega_r^2} = 73\,\mu$m, which is the spatial cutoff imposed by $\epsilon_{\rm cut}$. It thus has no other significant effect on the incoherent region. These parameters give an initial state containing $\sim 6\times10^5$ coherent-region atoms, with the remainder in the incoherent region.

There are some technical limitations of this approach. First, the number of atoms in the simulations is approximately constant due to the fixed chemical potential of the thermal reservoir, while the BEC number in the experiment first grows as T/T_c is reduced to ~ 0.6, then decays with a $1/e$ lifetime of 24(3) s. A related issue is the slow spatial drift of the barrier beam of the experiment, which can decrease the number of vortices that can be stably pinned to the barrier, providing a loss mechanism for the persistent current at long times; this latter aspect of our work will be discussed in a separate publication. However, our procedure is suitable for simulating the BEC conditions early in the stir and hold process, and we do not expect detailed modelling of the evaporative cooling stage to alter our main results.

Movie S1: Dynamics of a forced, damped BEC. This movie of the damped Gross-Pitaevskii equation dynamics may be viewed online at [URL to be provided by Physical Review]. The movie shows the column density and phase profile in the $z = 0$ plane generated for a simulation of the DPGPE for the experimental parameters. In the movie, small red circles in the phase profiles indicate vortices with circulation in the same sense as the stirring, while small blue crossmarks indicate vortices with opposite circulation. A number of events are visible, notably:

i) $t = 140$ ms: The first evidence of a boundary vortex appears at the *inside* boundary of the BEC. This is most apparent in the phase profile.

ii) $t = 160$ ms: A prominent density modulation feature develops.

iii) $t = 166$ ms: This time is half-way through stir sequence.

iv) $t = 190-210$ ms: The first vortices injected into the BEC via sound decay are visible.

v) $t = 220$ ms: Many vortices are now found in the bulk superfluid.

vi) $t = 230$ ms: Vortex dipole annihilation.

vii) $t = 260$ ms: Two long-lived vortex aggregates have formed (~3 o'clock and 4 o'clock positions).

viii) $t = 390$–410 ms: A vortex approaches the inner BEC boundary (~4 o'clock position) and is captured by the central barrier, increasing the circulation pinned to the barrier by one unit. In this process, a pulse of sound energy is emitted into the BEC.

ix) $t = 420$–450 ms: A vortex dipole forms as two vortices of opposite circulation approach each other (~ 7 o'clock position), then undergoes self-annihilation followed by revival at the outer BEC boundary.

x) $t = 480$–520 ms: A vortex dipole forms (~ 3 o'clock position), then undergoes self-annihilation followed by revival at the outer BEC boundary.

xi) $t = 590$–640 ms: A vortex dipole forms (~ 8 o'clock position), then undergoes self-annihilation followed by revival at the outer BEC boundary.

xii) $t = 600$ ms: Thermalization of the sound field across the whole system has occurred by this time.

xiii) $t = 790$ ms: Vortex dipole annihilation.

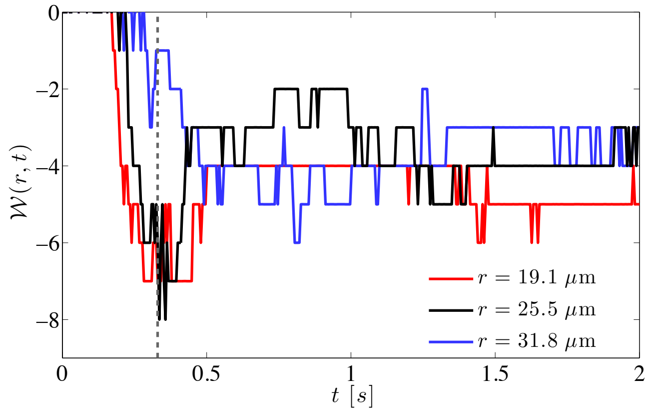

Figure S1. Winding number [Eq. (3)], for three radii, shown for the first 2 seconds of evolution after the beginning of the stir. The vertical dashed grey line indicates the end of the stir. The peak density of the initial state occurs at $r \sim 25\ \mu$m. The end-state of time evolution has $\mathcal{W} = -3$ at all radii.

xiv) $t = 1000$ ms: A two-vortex cluster, a dipole, and a free vortex collide. Vortex exchange occurs; the collision results in the same vortex structures emerging.

xv) $t = 1980$ ms: A vortex collision results in a vortex being slightly tilted with respect to the z axis (~ 4 o'clock position), showing that this system is not strictly two-dimensional. Note that this vortex returns to an orientation along the z axis within about 50 ms.

Development of large-scale flow. To quantify the development of large-scale flow from the initial small-scale forcing, we consider the winding number $\mathcal{W}(r,t)$ at a given radius r as a function of time t, as defined by

$$\mathcal{W}(r,t) = \frac{m}{h} \oint_r \mathbf{v}(\mathbf{r},t) \cdot \mathbf{dl}. \tag{3}$$

We plot this quantity for three radii, shown in Figure S1, for the first 2 seconds after the beginning of the stir. For the smallest radii, there is a an early injection of vortices due to the stir process. The vortices are nucleated near the inner boundary, with rapid increase in vortex nucleation occurring about half-way through the stir [see Figure S2]. At this point in time there is zero net winding number in the BEC, however angular momentum is being injected into the BEC, and is manifested by the preference for negatively charged vortices to accumulate at small radii and for the positively charged vortices to be distributed to larger radii. For the smallest radius shown in Figure S1, we see that the net charge within $19.1\,\mu$m of the BEC center begins a sequence of jumps up from 0 at ~ 181 ms, each jump to a larger negative number indicating that a positively charged vortex has moved outside of this inner region. Immediately after the end of the stir, $\mathcal{W}$ fluctuates around -6 for radii within about 25 μm, but for $r = 31.8\,\mu$m, $\mathcal{W}$ is near -1. Many vortices have moved outside of the inner regions by this time, but they have not reached the outer regions of the BEC. Thus at the end of the stir, superfluid flow at the largest scales of the system has not developed, and most of the circulation is concentrated in the BEC center. Over the next $\sim$ 150 ms, vortex motion occurs to bring $\mathcal{W}$ near -4 throughout the BEC, but significant fluctuations over the next 1.5 s indicate that steady large-scale flow has not been reached even by $t = 2$ s. Eventually, in the presence of damping, $\mathcal{W} = -3$ at all radii: this is the final persistent current state that is the signature of steady large-scale flow. This state is reached due to the net angular momentum directly injected by the stir *and* by the vortex dynamics and dispersal that occur after the end of the stir.

Forcing wavenumber analysis. We compute changes in total incompressible kinetic energy and enstrophy, ΔE^i and $\Delta\Omega$, during the interval from 181 ms to 208 ms after the start of the stir in order to estimate a forcing scale k_F, as described in the main text. These changes were computed by integrating the incompressible energy distributions (Fig. 3 of the main text) and the enstrophy distributions (obtained by multiplying $E^i(k)$ by k^2) for each of these two times, then taking their differences. We thus arrive at $k_F \equiv \sqrt{\Delta\Omega/\Delta E^i} = 0.57\xi^{-1} \simeq 2\pi/(11\xi)$, as stated in the main text.

Examining the instances of vortex dipole creation from sound during the stir period, we find dipole lengths d in the range 6.7ξ to 11ξ, suggesting an injection of incompressible energy near a wavenumber $k{\sim}2\pi/d$. At the vortex dipole annihilation event at $t = 230$ ms, the dipole length is $d{\sim}6.7\xi$. Two other transient events correspond to dipole annihilation, with dipole lengths of $\sim 6.7\xi$ and $\sim 8.9\xi$. Furthermore, the superfluid density modulations preceding vortex nucleation at the 181-ms spectral peak have a length scale of approximately $11\xi \simeq 2\pi/k_F$; see Fig. S2. Taken together, these observations indicate that forcing involves efficient energy and enstrophy transfer from the compressible to the incompressible fluid components for wavenumbers $k_F \lesssim k \lesssim k_s$.

An alternative view of the wavenumber range $k_F < k < k_s$ comes from considering the Jones-Roberts (JR) solitons of the two-dimensional GP equation [45]. JR solitons are localized excitations with group velocity v, and with characteristics that depend on the relationship of v to a critical velocity $v_c = 0.61c_s$, with c_s the sound velocity [45,46]. For $0 < v < v_c$ a JR soliton has an incompressible character, and appears in the fluid as a vortex dipole. For $v_c < v < c_s$ the JR soliton has a vortex-free compressible character, namely, an acoustic wave that appears as a short black or gray soliton. Using the de Broglie relation $\hbar k_F = mv_c$ to convert to an equivalent wavenumber yields $k_F = 2\pi/d$ with $d = 10.3\xi$, remarkably close to the value of $d = 11\xi$ obtained via distinct reasoning above and observed in our simulations. In a similar way the wavenumber associated with the sound velocity $v = c_s$ is $k_s = mc_s/\hbar = 1/\xi$. The wavenumber k_F thus emerges as that which delineates the boundary between nonlinear excitations of the 2D quantum fluid that are compressible and incompressible in character.

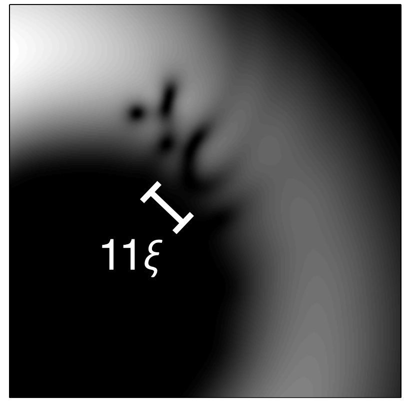

Figure S2. Numerically obtained column density 181 ms after stirring begins (see Movie S1). The bar indicates the scale of forcing calculated from the energy and enstrophy injected during the stir (see main text).

The wavenumber k_s is the maximum wavenumber of JR solitons. We thus physically expect that k_F and k_s will define a range of wavenumbers for which efficient exchange of kinetic energy between the compressible and incompressible components. Phenomenologically, this means that a vortex dipole whose vortices are separated by a distance within the corresponding range can efficiently self-annihilate and convert its incompressible energy into acoustic energy. The reverse process is also possible. We thus attribute this range to a wavenumber scale for forcing from the compressible component of the fluid into the incompressible component. This length scale, and its relationship to the interconversion of JR solitons between localized sound pulses and vortex dipoles, can be seen in the vortex dynamics of Movie S1.

Density modulations during forcing. Figure S2 shows the stir-induced density modulations observed in the simulations. These density modulations decay to vortices. As density modulations at a wavenumber k correspond to *compressible* energy at that wavenumber, we expect an influx of energy into the incompressible regime at a wavenumber that corresponds to these modulations, as discussed in the main text.

Experimental winding number determination. Multi-quantum vortices are energetically unstable, thus loose clustering is preferred to perfect co-location of multiple vortices. As in previous experiments [29,30], we make use of this energetic instability in order to determine the size of the persistent current formed and its subsequent time evolution in the experiment, as shown in Figure S3. By allowing additional hold time between beam ramp down and expansion, we can count the total number of free and pinned vortices for any hold time. For long-enough hold times where the number of free vortices has dropped to much less than one per image (on average), the observed vortices can be attributed to superflow around the central barrier, particularly if they appear clustered about the position of the barrier as

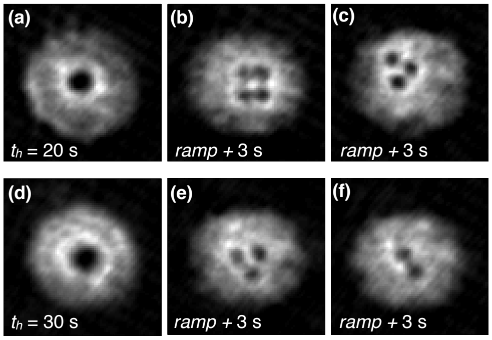

Figure S3. Vortices observed in experimental data. Here, BECs are held in the annular trap for 20 s prior to the central barrier ramp down, trap release, expansion, and imaging. In (a) the expansion and imaging procedure takes place immediately after the barrier ramp. The dark region in the center of the BEC corresponds to multiple units of circulation, and is not due to the presence of the barrier itself; i.e., with no circulation about the barrier, a hole would not appear in the BEC after ballistic expansion. In (b) and (c), BECs are held for an additional 3 s in the trap before the expansion imaging procedure. This additional hold time allows the vortices that comprise the region of vorticity shown in (a) to dissociate and become experimentally observable. (d)-(f) show similar images for t_h = 30 s.

shown in Fig. S3. We note that observations of such regular structures of vortices, as shown, do not always occur after beam ramp down, and the vortex distribution is often more irregular. As stated in the main text, the mean number of vortices experimentally observed at t_h = 23 s is 3.5. If instead we remove the central barrier at the *beginning* of the hold period, and let the system evolve in a purely harmonic trap for 23 s, the mean numbers of vortices observed becomes 1.2. The fluid circulation is thus maintained at significantly higher levels in the annular trap, supporting a description of this state as a persistent current.

Vortex clusters and dynamics. In Fig. 4 of the main text we show images from our simulations that contain evidence for vortex clusters that occur immediately before and after the completion of the stir in the annular trap. As a supplement to Fig. 4, Fig. S4 shows the corresponding phase plots. In these images, we make use of the vortex clustering algorithm described in Ref. [16]. The algorithm consists of two steps: (i) identifying all cases where vortices that are mutual nearest neighbors have opposite circulation, labeling these pairs as vortex dipoles, then removing them from further influence in later steps of the algorithm; (ii) identifying cases were vortices of the same circulation are closer to each other than to any opposite-circulation vortices; these vortices are grouped together in a cluster. These steps are repeated until no further correlations are possible. This algorithm for identifying clusters was specifically developed for homogeneous BEC systems, where healing lengths and hence vortex dimensions are uniform throughout the system. In this case, identification of vortices is not dependent on density, and the roles of boundary conditions do not influence vortex dynamics and vortex correlations. These issues can potentially cause difficulties in identifying clustering in trapped and multiply connected systems, but modifications to the algorithm for our annular, trapped BEC are beyond the scope of this work. Nevertheless we apply the algorithm to our data as a rough estimate of the degree of clustering that appears in our data. In doing so, we neglect vortices at the edges of the BEC or pinned to the central barrier that are not apparent in density plots.

Alternatively, we may examine the distribution of vortex clusters in the gas after the ramp down of the stirring potential to determine whether such clusters might also occur in the experimental system subsequent to beam ramp down, and to investigate the statistical robustness of vortex clusters in a different trap geometry after injection of the pinned vortices into the fluid. Clusters do indeed appear in such numerical data, as Fig. S5 shows. Here, the clustering algorithm is again applied, and two clusters with 5 vortices each are seen in the left-most plot, along with one 3-vortex cluster and two 2-vortex clusters. For these data, the fraction of vortices involved in same-circulation clusters is 0.73, 0.82, and 0.71 for times of 0, 100 ms, and 200 ms (respectively) after the end of the beam ramp-down. The mean circulation charge of the visible clusters is 4, 2.8, and 3.75, respectively. These statistics suggest that vortex pairing and clustering occur not by chance in a random distribution, but rather as signatures of developed 2DQT in the BEC.

We emphasize that vortex cluster measures are statistical, and are most meaningful when examined over time or under various realizations of a turbulent system. A cluster is not a dynamically stable unit, and can exchange vortices with the remaining vortex distribution, as well as lose or gain vortices. This makes cluster identification challenging to apply by visual inspection for all but the most tightly bound clusters or vortex pairs, and necessitates the use of a more quantitative analysis as is applied here.

Spherical trap simulations. For the numerical simulations investigating stirring in a spherical potential, the geometric mean trapping frequency and chemical potential were preserved, and the toroidal barrier width was chosen to preserve the hole width relative to the transverse Thomas-Fermi radius. The peak density is preserved by this rescaling, so that we also use the same stirring velocity.

* Current address: School of Mathematics and Physics, University of Queensland, Brisbane, Qld 4072, Australia
† Author to whom correspondence should be addressed; Email: abradley@physics.otago.ac.nz
‡ Author to whom correspondence should be addressed; Email: bpa@optics.arizona.edu
[39] C. W. Gardiner and M. J. Davis, J. Phys. B **36**, 4731 (2003).
[40] A. S. Bradley, C. W. Gardiner, and M. J. Davis, Phys. Rev. A **77**, 033616 (2008).

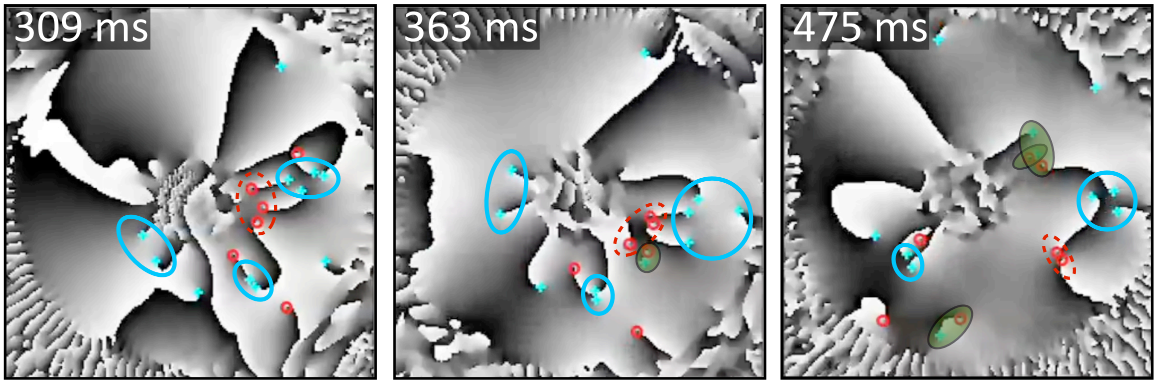

Figure S4. Phase plots corresponding to the density data of Fig. 4, main text. These plots are extracted from the right-hand panels of Movie S1 at the same times as the data of Fig. 4. As in the right-hand movie panel, quantum phase from $-\pi$ to π is represented by grayscale from black to white. In these images, small red circles indicate vortices with circulation in the same sense as the stirring, while small blue crossmarks indicate vortices with opposite circulation. Only vortices that are clearly distinguishable in the density distributions are indicated. See caption of Fig. 4 for additional description of figure elements.

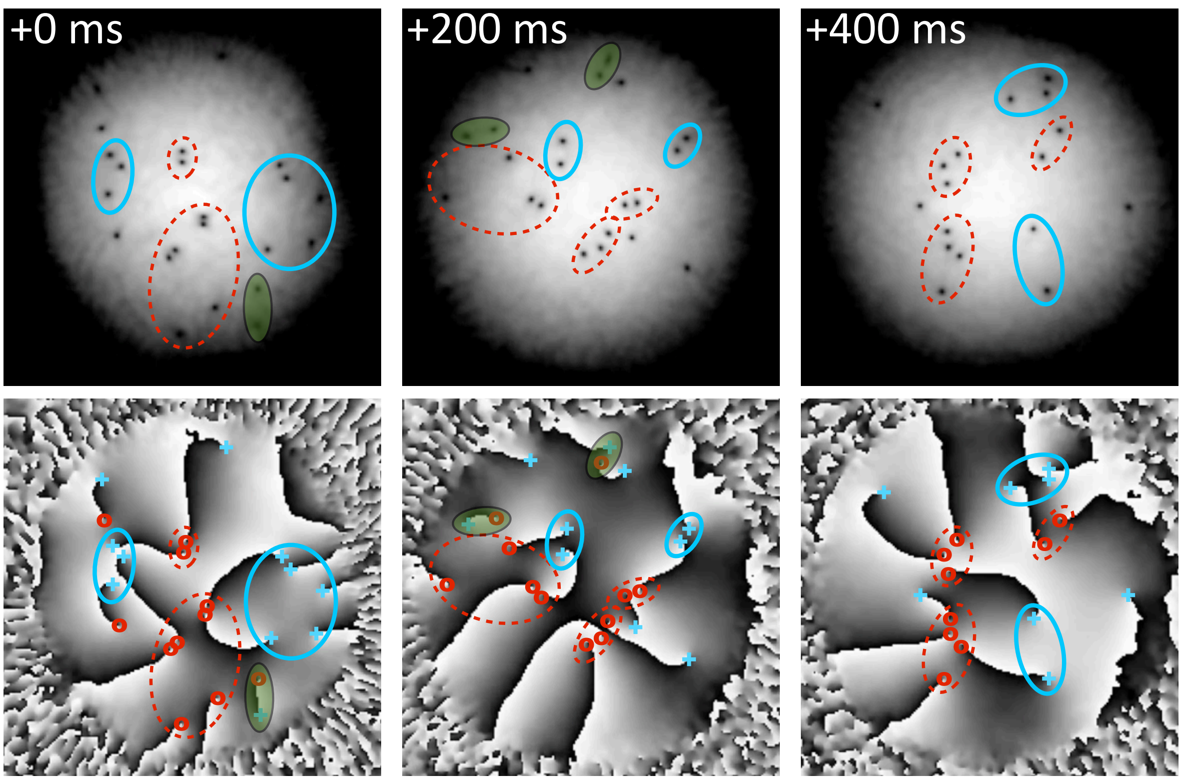

Figure S5. Density and phase plots showing vortex clusters seen for a main sequence hold time of $t_h = 0$ ms, followed by the 250-ms barrier ramp-down, and an additional hold time of 0 ms, 200 ms, and 400 ms (left to right) in the harmonic trap (96-μm-square images). See Fig. 4 of the main text and Fig. S4 for clarification of symbols.

[41] S. J. Rooney, P. B. Blakie, and A. S. Bradley, Phys. Rev. A **86**, 053634 (2012).
[42] S. J. Rooney, A. S. Bradley, and P. B. Blakie, Phys. Rev. A **81**, 023630 (2010).
[43] M. C. Garrett, T. M. Wright, and M. J. Davis, Phys. Rev. A **87**, 063611 (2013).
[44] S. J. Rooney, T. W. Neely, B. P. Anderson, and A. S. Bradley, arXiv:1208.4421.
[45] C. A. Jones, S. J. Putterman, and P. H. Roberts, J. Phys. A **19**, 2991 (1986).
[46] L. A. Smirnov and V. A. Mironov, Phys. Rev. A **85**, 053620 (2012).